MCB
Journals.ASM.org

Fidelity of Histone Gene Regulation Is Obligatory for Genome Replication and Stability

Prachi N. Ghule,[a,b] Rong-Lin Xie,[b] Ricardo Medina,[b] Jennifer L. Colby,[b] Stephen N. Jones,[b] Jane B. Lian,[a,b] Janet L. Stein,[a,b] Andre J. van Wijnen,[b]* Gary S. Stein[a,b]

Department of Biochemistry and Vermont Cancer Center, University of Vermont College of Medicine, Burlington, Vermont, USA[a]; Department of Cell Biology, University of Massachusetts Medical School, Worcester, Massachusetts, USA[b]

Fidelity of chromatin organization is crucial for normal cell cycle progression, and perturbations in packaging of DNA may predispose to transformation. Histone H4 protein is the most highly conserved chromatin protein, required for nucleosome assembly, with multiple histone H4 gene copies encoding identical protein. There is a long-standing recognition of the linkage of histone gene expression and DNA replication. A fundamental and unresolved question is the mechanism that couples histone biosynthesis with DNA replication and fidelity of cell cycle control. Here, we conditionally ablated the obligatory histone H4 transcription factor HINFP to cause depletion of histone H4 in mammalian cells. Deregulation of histone H4 results in catastrophic cellular and molecular defects that lead to genomic instability. Histone H4 depletion increases nucleosome spacing, impedes DNA synthesis, alters chromosome complement, and creates replicative stress. Our study provides functional evidence that the tight coupling between DNA replication and histone synthesis is reciprocal.

In both normal and tumor cells, DNA replication is functionally coupled to the activation of histone gene expression at the onset of S phase to support the packaging of newly replicated DNA as chromatin. Chromatin of eukaryotic cells consists of genomic DNA wrapped around an octamer comprised of two molecules of each of the four core histone subunits H2A, H2B, H3, and H4 to form the nucleosome, with one H4-H3 tetramer and two H2A-H2B dimers (1). Nucleosomes permit higher-order folding to ensure that total genomic DNA is functionally organized within the confines of the nucleus.

Histones are essential epigenetic proteins encoded by multiple genes (2, 3). The higher-order structure of chromatin plays a critical role in epigenetic regulation of gene expression that is linked to multiple posttranslational modifications of histones (e.g., lysine acetylation and methylation, arginine methylation, serine phosphorylation). Posttranslational modifications of histones and their role in DNA damage and repair have been studied extensively. It is also well established that there is tight coupling between levels of DNA and histone synthesis and that inhibition of DNA synthesis during S phase is responsible for rapid decline in histone synthesis (4–6). However, a key question is how perturbation of histone gene expression compromises the ordered replication and packaging of DNA in mammalian cells.

Histone H4 protein is the most highly conserved core nucleosomal protein. In human cells, there are 15 H4 histone genes that encode identical H4 proteins (1, 7, 8). Histone H4 gene expression is upregulated at the onset of S phase by transcriptional and posttranscriptional mechanisms to support synthesis of the vast quantities of H4 protein required for formation of nucleosomes during DNA replication (9–14).

Control of H4 gene expression during the cell cycle is mediated by transcription factor histone nuclear factor P (HINFP), a highly conserved Zn finger protein that binds to a conserved histone H4 promoter regulatory element (9, 15–17). Although a large number of histone gene transcription factors have been characterized, HINFP is unique because it is the only known histone H4 promoter-specific factor that interacts directly with the nuclear protein ataxia-telangiectasia locus (NPAT) (18, 19), an essential coactivator that in response to cyclin E/cyclin-dependent kinase 2 (CDK2) controls transcription of multiple histone genes (20–23). NPAT, along with HINFP, resides in subnuclear domains designated histone locus bodies (HLBs), where both histone gene transcription machinery and regulators of 3′-end processing of primary histone transcripts colocalize with histone genes (23–27). The HINFP-NPAT complex mediates a unique cell cycle regulatory mechanism that controls the G_1/S-phase transition (9, 18, 19, 28–30) and operates independently of the classical restriction point-related E2F/pRB switch. The biological significance of HINFP-mediated loss of histone H4 in cell cycle control is reflected by our earlier findings that a constitutive null mutation of the mouse *Hinfp* gene causes early embryonic lethality (31). *Hinfp*-null embryos exhibit a delay in hatching, abnormal growth, and loss of histone H4 gene expression (31). Thus, HINFP is a necessary CDK-dependent histone H4 gene regulator that, in contrast to the CDK2-cyclin E complex, cannot be compensated during embryogenesis (32, 33).

Because of the essential role for HINFP in cell cycle control of histone gene expression, deliberate loss of this factor permits assessment of the cell autonomous effects of histone H4 deficiency on cell growth and proliferation in mammalian cells. Therefore, we examined the mechanistic consequences of conditional inactivation of his-

Received 26 November 2013 **Returned for modification** 29 December 2013
Accepted 25 April 2014

Published ahead of print 5 May 2014

Address correspondence to Gary S. Stein, gary.stein@uvm.edu.

R.-L.X. and R.M. contributed equally.

* Present address: Andre J. van Wijnen, Departments of Orthopedic Surgery & Biochemistry and Molecular Biology, Mayo Clinic, Rochester, Minnesota, USA.

Supplemental material for this article may be found at http://dx.doi.org/10.1128/MCB.01567-13.

doi:10.1128/MCB.01567-13

tone H4 expression by selective elimination of the *Hinfp* gene. Our findings provide compelling evidence that diminished histone H4 expression alters both DNA replication and mitosis. Thus, the tight coupling between DNA replication and histone synthesis is reciprocal, and fidelity of histone gene regulation is necessary for chromatin integrity, genome replication, and stability.

MATERIALS AND METHODS

Generation of conditional *Hinfp* knockout mice. We targeted the mouse *Hinfp* locus by homologous recombination to generate conditional *Hinfp*$^{F/F}$ mice. Targeting of the *Hinfp* locus was confirmed by Southern blotting and PCR analysis. Animals were maintained according to Institutional Animal Care and Use Committee (IACUC) guidelines. Targeting vector was made with three genomic fragments, 2.5-kb left arm, 1.0-kb middle arm, and 5.2-kb right arm fragments, spanning introns 2 to 5, introns 5 to 9, and intron 9 to downstream of exon 10, respectively, that were generated by PCR using specific primer pairs from mouse AB2.1 genomic DNA (see Table S1 in the supplemental material) and cloned in tandem into the pGEM-5Zf(+) vector (Promega). We then inserted a 50-bp LoxP cassette between the left and middle arms, a 2.0-kb neomycin cassette flanked by Flp recombinase targets with a second LoxP site (Frt-PGKpromoter-Neo-Frt-LoxP) between the middle and right arms, and a 2.2-kb thymidine kinase gene cassette (PGKpromoter-TK) after the right arm. The Transgenic Animal Modeling Core at the University of Massachusetts Medical School provided the Neo and TK cassettes and electroporated the targeting vector into AB1 (129S7/SvEvBrd) embryonic stem (ES) cells. Two clones that correctly targeted the *Hinfp* locus were identified by Southern blotting and microinjected into C57BL/6J-Tyr[c-2J]/J mouse blastocysts. The *Hinfp*$^{FN/+}$ mice were generated by homologous recombination. We crossed *Hinfp*$^{FN/FN}$ with FLPeR mice (Jackson Laboratory stock number 003946) that express FLP1 recombinase driven by the Gt(ROSA)26Sor promoter to remove the Neo cassette and generate the true conditional *Hinfp*$^{F/F}$ mice (34).

Cell culture. U2-OS cells were propagated as recommended (ATCC). Mouse embryonic fibroblasts (MEFs) isolated at embryonic day 12.5/13.5 from wild-type (WT) and conditional *Hinfp*$^{F/F}$ embryos were cultured *ex vivo* and treated with an adenoviral vector coexpressing Cre recombinase and an enhanced green fluorescent protein (EGFP) marker for live-cell selection (Ad5CMVCre-EGFP; University of Iowa, Gene Transfer Vector Core) at passage 3. GFP-positive cells were sorted 36 h after infection (BD FACSAria I or II) and cultured. Samples were collected at sorting (day 0 [d0]) and/or at different time points (d1, d2, d3, d4) during culture.

Luciferase assay. U2-OS cells were seeded on 6-well plates at 0.8×10^5 to 1.0×10^5 cells/well, and transient transfections were performed using Fugene 6 (Roche). A total of 0.1 μg of pGL2WT-H4 promoter/luciferase (Luc) reporter and 5 ng of pGL2/*Renilla*-Luc control vectors were cotransfected with 0.1 μg of NPAT alone or 0.1 μg of NPAT with either 0.1 μg WT-*Hinfp* or mutant *Hinfp* (d6789-P) expression vectors. The total amount of DNA/well was kept constant by supplementing with the empty expression vector. Dual-luciferase reporter assays were performed 24 h after transfection. Firefly luciferase activity was normalized by *Renilla* luciferase reporter from three independent experiments.

EMSA. Electrophoretic mobility shift assay (EMSA) was performed as described earlier (17). Binding of mouse HINFP WT protein or a deletion mutant d6789-P was assessed with *in vitro* transcribed and translated (IVTT)-produced proteins with an Xpress tag. Oligonucleotides used were as follows: (i) an optimized HINFP binding site based on its recognition sequence in site II of the human H4/n gene, CTT CAG GTT TTC AAT CTG GTC CGA TAC T; (ii) mutated HINFP binding site, CTT CAG GTT TTC AAT CTT CTA CGA TAC T (mutated nucleotides are underlined); and (iii) a nonspecific competitor, ATT CGA TCG GGG CGG GGC GAG C. Oligonucleotides were labeled with [γ-^{32}P]ATP, and gels were analyzed by autoradiography. IVTT-produced HINFP proteins (WT and d6789-P) were also subjected to standard Western blotting protocol and immunodetected using a mouse monoclonal anti-Xpress antibody (1:5,000) (Invitrogen).

RNA isolation, cDNA synthesis, and real-time quantitative PCR (RT-qPCR). Total RNA from WT and *Hinfp* conditional knockout (cKO) MEFs was prepared using the miRNeasy Mini kit (Qiagen), and cDNA was synthesized with SuperScript First-Strand Synthesis System III (Invitrogen). Relative transcript levels were determined by the $\Delta\Delta C_T$ method using cycle threshold (C_T) obtained in a 7300/Viia 7 real time PCR system (Applied Biosystems) and iTaq SYBR green supermix with ROX (Bio-Rad Laboratories). Primer sequences are listed in Table S2 in the supplemental material.

Western blotting. Proteins were isolated from whole-cell lysates of WT and cKO MEFs with no infection or post-GFP sorting (d0 to d4) using RIPA buffer with protease inhibitor cocktail (Roche) as per standard protocols. The proteins were subjected to standard Western blotting protocol and immunodetected using specific antibodies. Antibodies were total H4 rabbit polyclonal (1:10,000; Abcam), alpha-tubulin mouse monoclonal (1:10,000; Sigma), cyclin D1 mouse monoclonal (1:1,000; Zymed), cyclin E rabbit polyclonal (1:1,000; Santa Cruz), cyclin A rabbit polyclonal (1:1,000; Santa Cruz), cdc2/CDK1 mouse monoclonal (1:1,000; Santa Cruz), and CDK2 rabbit polyclonal (1:1,000; Santa Cruz) antibodies.

Immunofluorescence. GFP-sorted MEFs (WT and cKO) were cultured on coverslips for up to 4 days, and samples were collected at d1, d2, and d4. Immunofluorescence (IF) was carried out as described previously (24). Antibodies used for IF were anti-Xpress mouse monoclonal (1:1,000; Invitrogen), NPAT mouse monoclonal (1:1,000; BD Biosciences), alpha-tubulin mouse monoclonal (1:500; Sigma), Ki67 rabbit polyclonal (1:200; Abcam), γ-H2AX-S139 mouse monoclonal (1:250; Millipore/Cell Signaling), and 53BP1 mouse monoclonal (1:250; Santa Cruz) antibodies.

Fluorescence *in situ* hybridization. Oligonucleotide probes (prelabeled with biotin) specific for major or minor satellite regions of the mouse chromosomes were generously provided by Jeanne Lawrence (University of Massachusetts [UMASS], Worcester, MA). Fluorescence *in situ* hybridization (FISH) was performed on WT and cKO MEFs arrested at mitosis with 100 ng/ml colcemid (Invitrogen) at d2. The hybridization and detection were carried out as described previously (35).

For both IF and FISH, cells were viewed under an epifluorescence Zeiss Axioplan 2 or Zeiss AxioImager microscope equipped with a Hamamatsu charge-coupled device (CCD) camera. Images were analyzed by either Metamorph imaging software (Universal Imaging) or by Zen 2011 imaging software (Zeiss). Images were captured at ×200, ×400, ×630, or ×1,000 magnification unless noted otherwise.

Senescence-associated β-galactosidase staining. Both WT and *Hinfp*-null MEFs grown in culture for 2 to 4 days after GFP sorting were stained for senescence-associated β-galactosidase (SA β-Gal) according to the protocol of Dimri et al. (36), with slight modifications. The stained cells were viewed under a bright-field Zeiss Axioskop microscope equipped with a SPOT camera, and images were captured using Axiovision software.

BrdU incorporation. Incorporation of 5-bromo-2′-deoxyuridine (BrdU) (Roche) into WT and cKO MEFs grown on coverslips was examined by pulse-labeling for 30 min at 37°C at d1, d2, and d4. Cells were then processed as per the manufacturer's protocol and visualized by IF microscopy. Percentage of S-phase cells (BrdU positive) was determined by counting 200 nuclei per sample from two biological replicates. Error bars represent standard errors of the means (SEM).

Premature chromosome condensation. WT and cKO MEFs (GFP sorted) were treated with 50 nM calyculin A (Sigma) to induce premature chromosome condensation (PCC; as described in reference 37). Fixed PCC cell suspension was dropped onto glass slides, and DNA was stained with 4′,6-diamidino-2-phenylindole (DAPI) for microscopic analysis.

Digestion of nuclei with MNase. Nucleosome repeat length was assessed by digestion of WT and *Hinfp* cKO MEF nuclei (d4 after sorting) with micrococcal nuclease (MNase) (NFCP; Worthington Biochemical Corp). Briefly, nuclei were isolated by Dounce homogenization of cells in ice-cold RSB buffer (10 mM Tris-HCl [pH 7.4], 10 mM NaCl, 5 mM $MgCl_2$) supplemented with 0.5% Nonidet P-40. Nuclei were recovered by centrifugation at

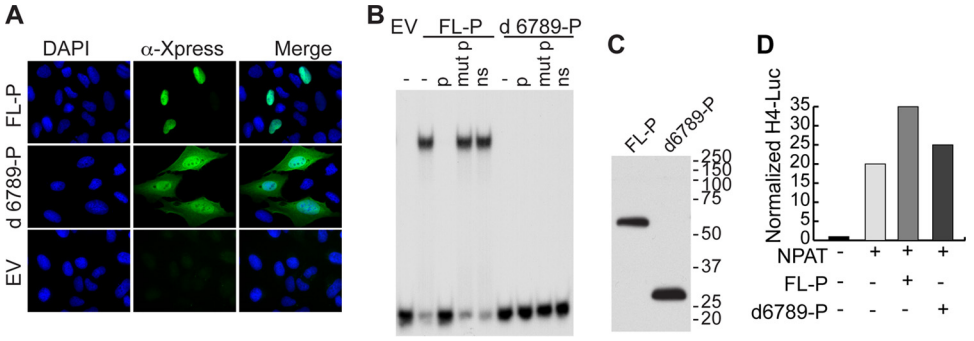

FIG 1 Functional characterization of conditional HINFP mutant protein *in vitro*. (A) IF microscopy of U2-OS cells transfected with Xpress-tagged HINFP expression vectors: full-length (FL-P) mouse HINFP, mutant HINFP (d6789-P) lacking exons 6 to 9, and empty vector (EV). The d6789-P mutant HINFP protein is mislocalized. (B) EMSA using IVTT proteins generated from the vectors described above shows mutated HINFP (d6789-P) lacks DNA binding: lane 1, EV; lanes 2 to 5, FL-P; and lanes 6 to 9, d6789-P with or without competitor (100×) oligonucleotides. (C) Western blot analysis of IVTT proteins: lane 1, full-length HINFP protein; lane 2, d6789-P HINFP protein lacking exons 6 to 9. (D) Relative luciferase activity of wild-type histone H4n/L promoter was measured after cotransfection with NPAT alone or NPAT with WT or mutated HINFP. The mutated HINFP reduces NPAT-associated activity of histone H4 promoter elements.

1,000 × *g* for 5 min at 4°C, washed twice with ice-cold RSB buffer, and recovered by centrifugation as described before. Nuclei were then suspended in RSB buffer supplemented with 1 mM $CaCl_2$ and incubated with increasing concentrations of MNase for 5 min at room temperature with gentle agitation; reactions were stopped by the addition of EDTA-EGTA buffer (25 mM EDTA and 10 mM EGTA; pH 8.0). DNA was purified by standard phenol-chloroform-isoamyl alcohol extraction and electrophoresed in 1.5% agarose gels. Images were analyzed using ImageJ software.

DNA fiber assay. WT and cKO MEFs (GFP sorted) at d2 and d4 were subjected to sequential pulse-labeling with thymidine analogs iododeoxyuridine (IdU) and chlorodeoxyuridine (CldU) (30 min and 20 min, respectively) at 10 μg/ml. The DNA fiber assay was performed as previously described (38, 39), with slight modification. DNA fibers were obtained by spreading the lysed cells onto a glass slide. Spread DNA fibers were fixed and immunostained with anti-BrdU mouse monoclonal antibody (BD Biosciences) for IdU and anti-BrdU rat monoclonal antibody (Abcam) for CldU, detected with appropriate fluorescence-tagged secondary antibodies, and analyzed by IF microscopy.

RESULTS

Conditional ablation of histone H4 gene transcription factor HINFP compromises cell proliferation. To address the cell autonomous function of HINFP, we constructed a nonfunctional mutant mouse allele that expresses a C-terminally truncated, DNA binding-defective, and inactive transcription factor (Fig. 1). Homologous recombination of the targeting construct in mouse ES cells generated a conditional knockout (cKO) allele in which exons 5 through 9, encoding multiple essential Zn fingers, were flanked by *loxP* sites (Fig. 2A and B). *Ex vivo* cultures of mouse embryonic fibroblasts (MEFs) derived from wild-type and homozygous *Hinfp* cKO embryos were infected with an adenovirus coexpressing Cre recombinase and enhanced green fluorescent protein (EGFP) marker. Cre-mediated recombination of the *loxP* sites resulted in the predicted shortening of the corresponding region within both *Hinfp* alleles (Fig. 2C). This genomic ablation generated truncated *Hinfp* gene transcripts (Fig. 2D) and caused 50% reduction in expression of H4 mRNA at d0, which was further reduced (~90%) by d4 (Fig. 2E). Analysis of effects of *Hinfp* ablation on other histone genes revealed an early compensatory increase in mRNA expression of H3, H1, H2A, and H2A.Z on d0 and d1, while H2B increased at later times (see Fig. S1 in the supplemental material). Importantly, total histone H4 protein levels showed ~50% reduction at d2 onward in the *Hinfp*-ablated cells (Fig. 2F; see also Fig. S2 in the supplemental material). Thus, ablation of *Hinfp* compromises histone H4 expression.

We investigated the phenotypic effects of *Hinfp* deficiency on cell growth. Wild-type MEFs with or without Cre expression, as well as cKO cells without Cre expression, proliferated rapidly, while *Hinfp* cKO cells in which the floxed allele was ablated by Cre expression exhibited compromised cell proliferation (see Fig. S3 in the supplemental material). These results were corroborated using wild-type and *Hinfp*-null MEFs sorted by flow cytometry using the EGFP fluorescent marker (Fig. 3A). Loss of *Hinfp* prevented an increase in cell number, either by inhibiting cell growth and/or increasing cell death. Cell cycle analysis by fluorescence-activated cell sorting (FACS) showed an increased percentage of cells with less-than-diploid (<2n) DNA content, consistent with cell death in *Hinfp*-null cells (Fig. 3B). Interestingly, FACS analysis also showed that *Hinfp*-depleted MEFs had a substantially increased fraction of polyploid cells (4n or 8n), while WT MEFs maintained normal cell cycle distribution (Fig. 3B). To confirm alterations in cell proliferation, we examined expression of many cell cycle-associated factors, such as cyclins A, E, and D, CDKs, and CKIs. WT and cKO MEFs showed no change in expression of cyclins A or E, CDK1, or cMyc, while there was increased expression of CDK2, cyclin D1, and p21 and p53, and expression of p27 decreased at d4 in cKO cells (see Fig. S1 and S2 in the supplemental material). The changes in cell cycle regulatory factors confirm our findings of a proliferation defect due to ablation of *Hinfp*. Furthermore, *Hinfp*-null cells showed an increased staining for senescence-associated β-galactosidase (SA β-Gal) (Fig. 3C). Thus, ablation of *Hinfp* causes cell autonomous proliferation defects.

HINFP supports the subnuclear organization and transcription of histone genes through its interactions with histone H4 gene promoters and recruitment of its coactivator NPAT, a resident protein of HLBs (NPAT foci). Loss of Hinfp altered the number and distribution of HLBs. Rather than forming a limited number of distinct NPAT foci per nucleus as in wild-type cells (2 to 4 foci), many *Hinfp*-deficient MEFs (70 to 75% cells) exhibited aberrant NPAT staining, with either a diffuse, nonfocal pattern of distribution or the presence of multiple foci (8 to 12 foci) (Fig. 3D and E). The diffused appearance of NPAT may reflect disorganization of HLB formation, while an increased number of NPAT foci is consistent with the polyploid phenotype. Hence, inactivation of *Hinfp*

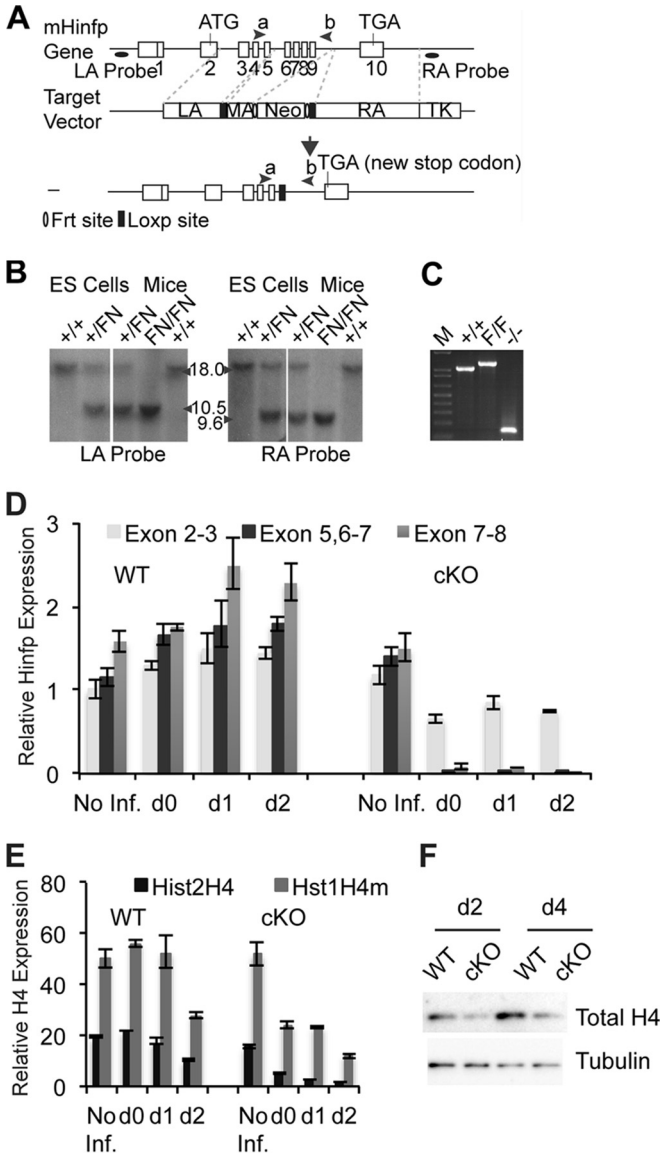

FIG 2 Conditional ablation of transcription factor HINFP inactivates histone H4 expression. (A) Schematic diagram showing targeted *Hinfp* locus to generate conditional *Hinfp* knockout mice. The arrow indicates the recombined locus that generates a conditional *Hinfp*-null mutation (−, null). Ovals indicate right- and left-arm probes for Southern blotting. Arrowheads represent genotyping primers for PCR. (B) Autoradiographs of Southern blot analysis of mouse ES cell clones (wild type [+/+] and +/FN) and mouse tail DNA (+/FN, FN/FN, and +/+) that were hybridized to either left- or right-arm probes: 18.0-kb WT allele and either 10.5-kb (LA probe) or 9.6-kb (RA probe) targeted allele. (C) PCR genotyping analysis of DNA from MEFs of wild-type (+/+) and *Hinfp*-null pups (F/F) with or without infection with Ad5CMVCre-EGFP virus using primers a and b shown in panel A. Lane 1, marker; lane 2, WT MEFs; lane 3, F/F MEFs without Cre infection; and lane 4, *Hinfp*-null MEFs after Cre treatment. (D and E) RT-qPCR analysis of WT and cKO MEFs without (No Inf.) or with Cre infection (d0 to d2) showing expression of *Hinfp* mRNA for multiple exons (exons 2-3, 5, 6-7, 7-8) (D) and two histone H4 genes (*Hist2H4* [H4] and *Hist1H4m* [H4m]) (E). Removal of *Hinfp* causes a marked decrease in histone H4 gene expression. (F) Western blot analysis of WT and cKO MEFs at d2 and d4 shows reduction of total H4 protein in *Hinfp*-null cells (see also Fig. S2 in the supplemental material).

alters the subnuclear microenvironment that normally controls histone gene expression at HLBs.

Proliferation defects in *Hinfp*-null cells are associated with aberrant nuclear and chromosomal phenotypes. We further examined the altered cellular phenotypes caused by *Hinfp* deficiency. Immunofluorescence (IF) microscopy of MEFs in which both *Hinfp* alleles were excised revealed clear changes in nuclear morphology (Fig. 4). Nuclear staining of *Hinfp*-deficient MEFs with DAPI showed that nuclei were larger than those of WT MEFs, and a fraction of the cKO cells had features consistent with fused or apoptotic nuclei (Fig. 4A). FACS data from WT and cKO MEFs also indicated an increase in cell size consistent with increased DNA content and larger nuclei (see Fig. S4A in the supplemental material). Further analysis of nuclear and cellular morphology by staining for alpha-tubulin revealed an increase in the number of binucleated cells in *Hinfp*-deficient MEFs (d1, 11% ± 2.8%; d2, 19% ± 1.4%; d4, 43% ± 6.4%) compared to that of the wild type (d1, 3% ± 1.2%; d2, 5% ± 1.5%; d4, 8% ± 2.5%) (Fig. 4B).

To assess changes in chromosome complement, cells were mitotically arrested, and DNA-FISH analysis was carried out using probes that detect the major and minor satellite regions on mouse chromosomes (Fig. 4C). Analysis of chromosome spreads showed major differences in the number of chromosomes in *Hinfp*-null MEFs (~60% mitotic cells with >2n) compared to wild-type MEFs (~20%); null cells appear to have three to four times the normal chromosome complement (Fig. 4C and D). The increase in nuclear size, presence of binucleated cells, and change in chromosome complement prompted us to investigate mitosis in more detail by alpha-tubulin staining of mitotic spindles. In asynchronously dividing populations, *Hinfp*-null cells exhibited the presence of multipolar spindles in 16 of 19 observed mitoses at d2 (Fig. 4E); two of the three remaining mitoses showed bipolar spindles that had atypical arrangements of chromosomes at the metaphase plate (see Fig. S4B in the supplemental material). Taken together, these abnormal nuclear, cellular, and mitotic phenotypes corroborate the data from FACS analysis that ablation of *Hinfp* results in disrupted ploidy and renders mitosis and cytokinesis defective.

Disruption of histone H4 expression impairs DNA synthesis and alters nucleosome spacing. Because *Hinfp* primarily supports the synthesis of histone H4 protein during S phase, we postulated that polyploidy may originate from deregulation of the tight coupling between DNA synthesis and histone deposition on newly replicating DNA. Histones are among the most abundant nuclear proteins synthesized during S phase, and inhibition of H4 protein synthesis may interfere with DNA synthesis. To understand interphase-specific effects of *Hinfp* ablation on cell cycle progression, we first monitored the presence and appearance of the proliferation-specific marker protein Ki-67, which exhibits distinct focal staining patterns at different cell cycle stages (40, 41). Ki-67 staining revealed a modest change in the fraction of S-phase cells (i.e., 49% and 58% at d4 in *Hinfp*-null and wild-type cells, respectively; Fig. 5A and B). There was also an increase in the population of quiescent (G_0) cells that lack Ki-67 staining (44% in *Hinfp*-null cells versus 27% in wild-type cells). Thus, loss of *Hinfp* reduces the fraction of actively dividing cells.

The small reduction in the S-phase fraction of *Hinfp*-null cells was unexpected given the obvious cellular and chromosomal aberrations observed. Furthermore, growth curve analysis of *Hinfp*-deficient cells (Fig. 3) indicated a severe delay in proliferation, contrary to the presence of a substantial S-phase fraction detected

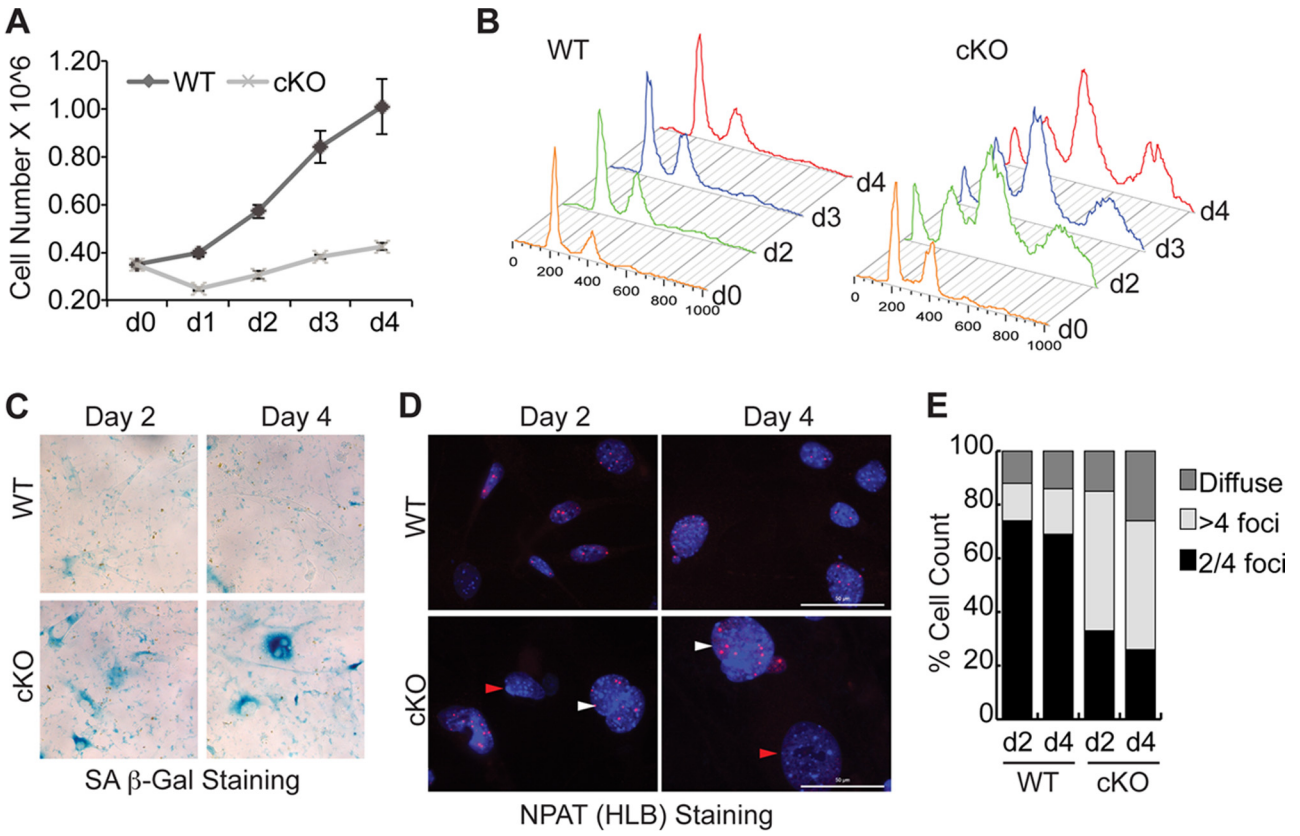

FIG 3 Loss of *Hinfp* causes deregulation of cell proliferation. WT and cKO MEFs (GFP sorted) were cultured for 4 days. (A) WT and cKO MEFs plated at 0.35×10^6/60-mm dish were harvested at different time points (d0 to d4) to analyze proliferation in culture. cKO cells show severe delay in proliferation. (B) Cell cycle analysis by flow cytometry for DNA content shows increased sub-G_1 population, altered S phase, as well as polyploid cells in cKO MEFs. (C) Senescence-associated β-galactosidase (SA β-Gal) activity was measured at d2 and d4. There is an obvious increase in SA β-Gal-specific staining in cKO MEFs that is enhanced at d4. (D) The distribution of HLBs was determined by staining for NPAT (red). IF microscopy revealed an increase in the fraction of cells with multiple NPAT foci (white arrowheads) or diffused NPAT staining (red arrowheads) in cKO MEFs at d2 and d4. The nuclei were counterstained with DAPI (blue). Scale bar, 50 μm. (E) Quantitation of NPAT staining patterns in WT and cKO MEFs at d2 and d4. Bar graph shows the percentage of cells with specific numbers of NPAT foci. A total of 200 nuclei were counted from two biological replicates per sample for each time point.

by Ki-67 staining. To investigate the apparent inconsistency between the S-phase fraction and cell division rate of *Hinfp*-null cells, we measured DNA synthesis in cultures of *Hinfp*-null and wild-type MEFs by pulse-labeling with bromodeoxyuridine (BrdU). Immunofluorescence microscopy revealed a severe reduction in BrdU-labeled nuclei in *Hinfp*-ablated cells compared to that in wild-type cells at d4 (Fig. 5C and D). The persistence of cells with an S-phase-specific Ki-67 pattern, together with a reduction in the number of cells incorporating BrdU, indicates that absence of *Hinfp* significantly inhibits active DNA synthesis, impedes S-phase progression, and creates a cell cycle defect.

To confirm alterations in DNA synthesis and cell cycle progression, we next examined interphase chromatin of wild-type and *Hinfp*-null MEFs by premature chromosome condensation (PCC) assay. This assay uses the protein phosphatase C inhibitor calyculin A to force chromosomes to condense during interphase and thus allows visualization of cell cycle stage-specific PCC patterns (37, 42). PCC patterns in *Hinfp*-deficient MEFs and WT MEFs were analyzed by counting 100 cells each with premature chromosome condensation at d2 and d4. The wild-type cells showed an S-phase-specific PCC pattern in 31% ± 0.7% at d2 and 30% ± 4.2% at d4, whereas cKO cells had 67% ± 0.8% at d2 and 65% ± 2.5% at d4 (Fig. 5E). Thus, *Hinfp*-null cells appear to be blocked in S phase. This S-phase-specific defect, as well as results from Ki-67 and BrdU staining, indicates that loss of *Hinfp* perturbs the cell cycle by interfering with DNA synthesis.

Histone proteins are normally present in S phase to package newly replicated DNA. Deletion of the *Hinfp* locus diminishes histone H4 gene expression (Fig. 2E), and the resulting decrease of newly synthesized histone H4 proteins may reduce deposition of histone H4 into nucleosomes. To test this hypothesis, we performed micrococcal nuclease digestion of nuclei from wild-type and conditional *Hinfp*-null cells. The average repeat length in wild-type MEFs was 209 bp, consistent with the average ~200-bp nucleosome spacing observed in many different cell types (reviewed in references 43 and 44). However, there was a marked increase in nucleosome repeat length in *Hinfp*-null cells (250 bp), reflecting an ~20% increase in nucleosome spacing throughout the genome (Fig. 5F). Thus, histone H4 deficiency reduces packaging of DNA into chromatin and may compromise genome integrity and predispose to chromosome instability.

***Hinfp*-mediated histone H4 deficiency stalls replication forks and increases double-stranded DNA damage.** Our cumulative evidence indicates that loss of *Hinfp* creates global

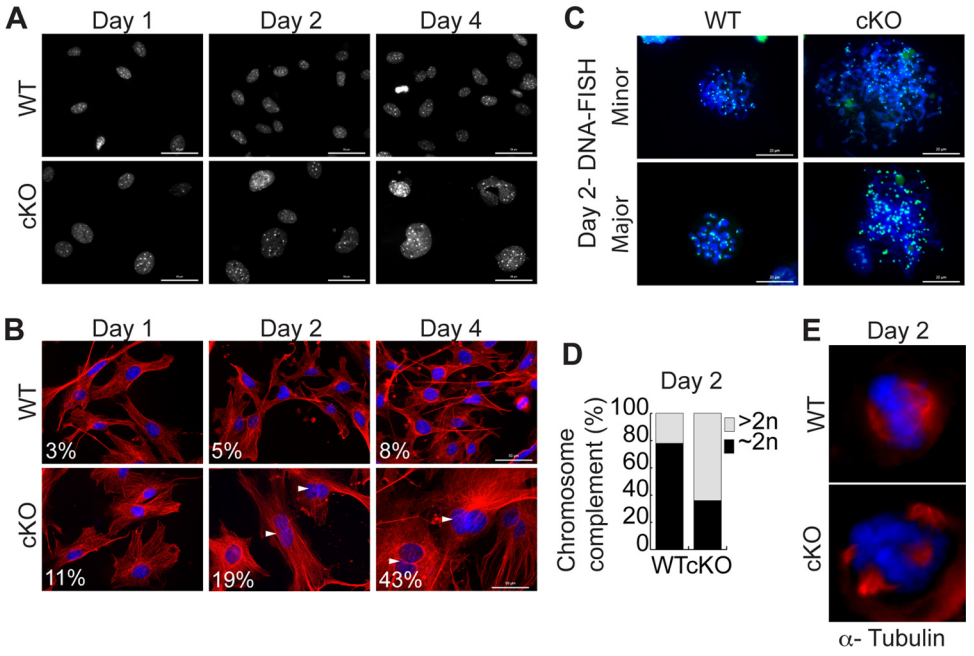

FIG 4 *Hinfp* ablation results in atypical nuclear and chromosomal morphology. WT and cKO MEFs (post-GFP sorting) were harvested at d1, d2, or d4 in culture. (A) IF microscopy shows obvious differences in nuclear size and shape between WT and cKO MEFs from d2 onwards. Nuclei stained with DAPI (gray) show clear increase in size after removal of *Hinfp*. Scale bar, 50 μm. (B) IF microscopy of MEFs stained with α-tubulin (red) show increased presence of binucleated cells (arrowheads) in cKO MEFs. The insets indicate percentage of binucleate cells. Scale bar, 50 μm. (C) Mitotic preparations of MEFs at d2 were subjected to DNA-FISH with probes against mouse minor satellite (top) or major satellite (bottom) regions. *Hinfp*-ablated cells show obvious increase in the chromosome complement. Scale bar, 20 μm. (D) Quantitation of mitotic cells from WT and cKO MEFs at d2 probed with satellite DNA was performed to calculate percent distribution of diploid (~2n) and polyploid (>2n) chromosome complement. A total of 50 metaphases were counted per sample. The bar graph shows higher percentage of polyploidy in cKO MEFs than in WT MEFs. (E) The microtubules of asynchronous WT and cKO MEFs at d2 were stained with α-tubulin (red) and analyzed by IF microscopy. The micrograph shows the presence of mitotic cells with multipolar spindles in cKO MEFs.

genomic defects, especially during S phase. Therefore, we investigated whether loss of *Hinfp* increases mechanistic markers associated with DNA damage. We examined γ-H2AX foci (phosphorylation of H2AX at S-139) and 53BP1 foci that represent DNA double-strand break regions phosphorylated by the ataxia telangiectasia-mutated (ATM) kinase (45–47). *Hinfp*-null cells exhibited an increased presence of γ-H2AX staining with both larger and more intense foci than those of WT cells (Fig. 6A). Similarly, homozygous deletion of the *Hinfp* locus resulted in redistribution of the normally diffuse nuclear organization of 53BP1 into the DNA damage-associated focal pattern (Fig. 6B). Hence, two different markers associated with DNA damage indicate that loss of *Hinfp* generates double-strand DNA breaks.

Evidence of double-strand DNA breaks and severe S-phase defects due to loss of *Hinfp* and associated deficiency of histone H4 and nucleosomes indicated replication stress and warranted detailed analysis of the consequences of *Hinfp* ablation on DNA replication. We monitored DNA replication directly using the DNA fiber assay, which employs sequential pulse-labeling with the thymidine analogs iododeoxyuridine (IdU) and chlorodeoxyuridine (CldU) to assess DNA replication fork progression. The incorporation patterns showed that *Hinfp*-null cells had a substantially increased percentage of stalled replication forks compared to that of wild-type cells (Fig. 6C and D). Thus, *Hinfp* deficiency and resulting absence of histone H4 block progression of DNA replication forks. While the principal combined cellular effect of *Hinfp* ablation is extensive changes in genomic integrity during interphase and mitosis, our results demonstrate a root cause of this cellular phenotype is the S-phase-specific perturbation of DNA replication.

DISCUSSION

In this study, we establish that ablation of histone H4 transcription factor HINFP generates replicative stress and causes striking cellular changes during both active DNA synthesis and mitosis. Because histone H4 genes are primary targets of *Hinfp*, the fidelity of genome replication directly depends on the *Hinfp*-mediated *de novo* production of histone H4 mRNAs and proteins to package DNA during S phase. Thus, *Hinfp* is functionally important for maintenance of genome integrity during normal cell cycle progression and mammalian development.

Conditional ablation of *Hinfp* as a model for epigenetic insufficiency. Histone H4 protein is the most highly conserved core octamer protein of the nucleosome and is subjected to multiple posttranslational modifications that support epigenetic control of transcription. There is considerable interest in examining the biological importance of histone H4 proteins in controlling transcription. However, it is technically challenging to mutate the total histone H4 complement in mammals because multiple, highly similar gene copies encoding H4 protein are located in broad genomic clusters on multiple chromosomes (16). The data presented here indicate that conditional *Hinfp*-null mutation can be used with Cre-mediated excision to render cells acutely deficient of H4 mRNA. Importantly, this approach can be applied to investigate H4 deficiency in multi-

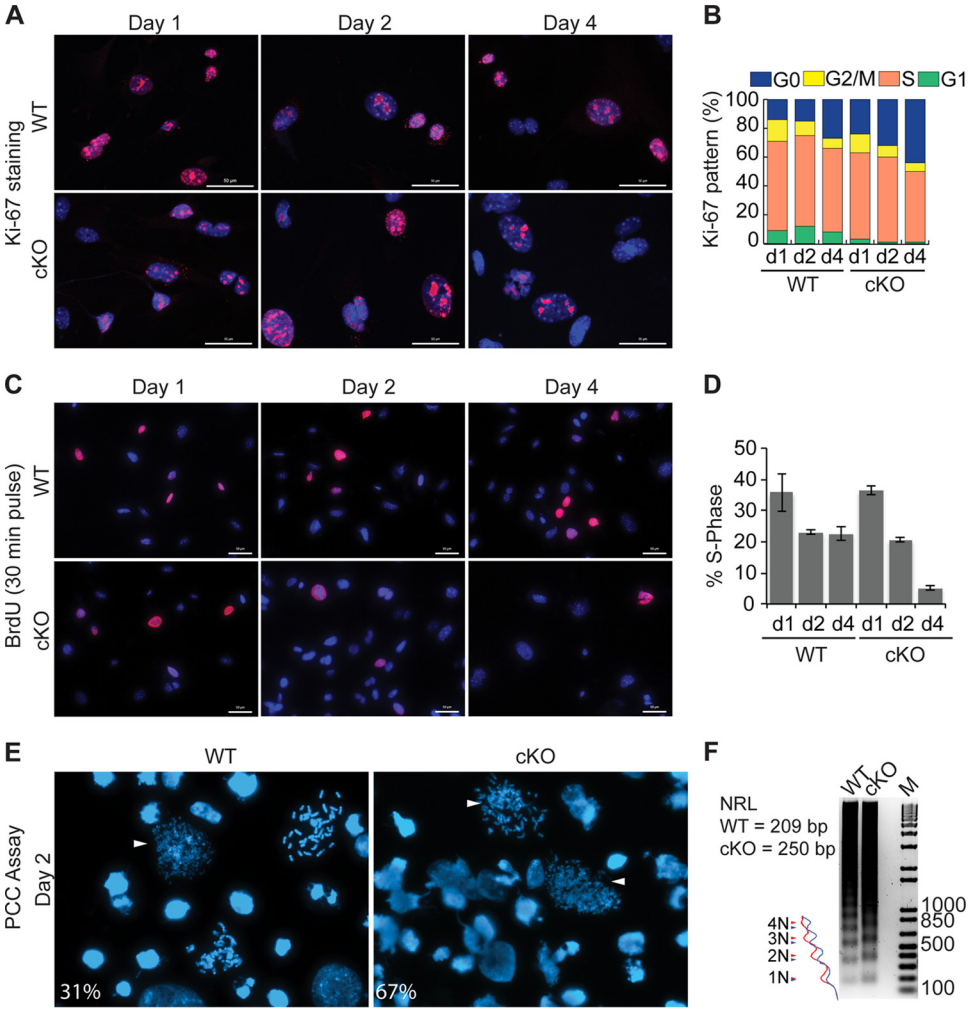

FIG 5 Loss of *Hinfp* causes S-phase delay. (A) IF staining of Ki-67 (red) as the cell cycle marker was carried out on WT and cKO MEFs. The nuclei were counterstained with DAPI (blue). Scale bar, 50 μm. (B) Quantitation of different Ki-67 patterns revealed that *Hinfp*-null MEFs show a higher percentage of G_0 cells and persistence of cells with the S-phase pattern. (C) Active DNA synthesis was measured by pulse-labeling of WT and cKO MEFs with BrdU (red). cKO cells at d4 show a substantial decrease in BrdU incorporation. Scale bar, 50 μm. (D) Quantitation of percentage of S phase (BrdU-positive cells) shows a marked decrease in active DNA synthesis (5% in cKO versus 21% in WT) at d4. A total of 400 nuclei were counted from two biological replicates for panels B and D. (E) WT and cKO MEFs were subjected to drug-induced PCC assay. DNA was stained with DAPI (blue). A higher incidence of S-phase-specific (arrowheads) PCC pattern was observed in cKO MEFs. Insets indicate percentage of S-phase-specific PCC patterns. (F) Nucleosome repeat length (NRL) assay of MEF DNA at d4 shows differences in the nucleosome ladder by gel electrophoresis. The images were analyzed using ImageJ software. Line scan analysis revealed broadening of bands and increased nucleosomal spacing in cKO MEFs.

ple cell lineages by selective expression of promoter-driven Cre. Furthermore, *Hinfp*-null cells are a powerful model system to examine the capability of different histone H4 mutants to rescue cells from the deleterious effects of *Hinfp* deficiency. This approach may also be applicable to genetic suppression of other multigene families that are controlled by a unique master regulatory transcription factor.

Catastrophic cellular and molecular consequences of *Hinfp*-mediated histone H4 deficiency. Here, we have defined multiple cellular and molecular phenotypes triggered by the loss of *Hinfp* and consequential reduction in H4 RNA and protein expression. The observed global genomic increase in nucleosome spacing upon *Hinfp* ablation reflects insufficient availability of newly synthesized histone H4 during DNA replication. This histone H4 deficiency will impede assembly of new nucleosomes. Deregulation of the normal H4 protein deposition at points of DNA synthesis may decelerate progression of and/or cause stalling of replication forks. Such *Hinfp* deficiency-related replicative stress is likely to induce genomic instability and DNA damage during S phase. Several studies in yeast have shown that removal or altered dosage of other core nucleosomal proteins H3 and H2B in addition to H4 creates numerous cell growth defects, increased sensitivity to DNA damage, and altered nucleosome positioning (48–55). Recent findings also show that perturbations in normal nucleosome spacing compromise transcription and genome integrity, as well as predispose dividing cells to tumorigenesis (56). Our findings in mammalian cells are consistent with the studies in yeast and establish that deficiency of histone H4 mRNA alters DNA replication and increases genomic stress.

Compromised DNA replication and accompanying damage

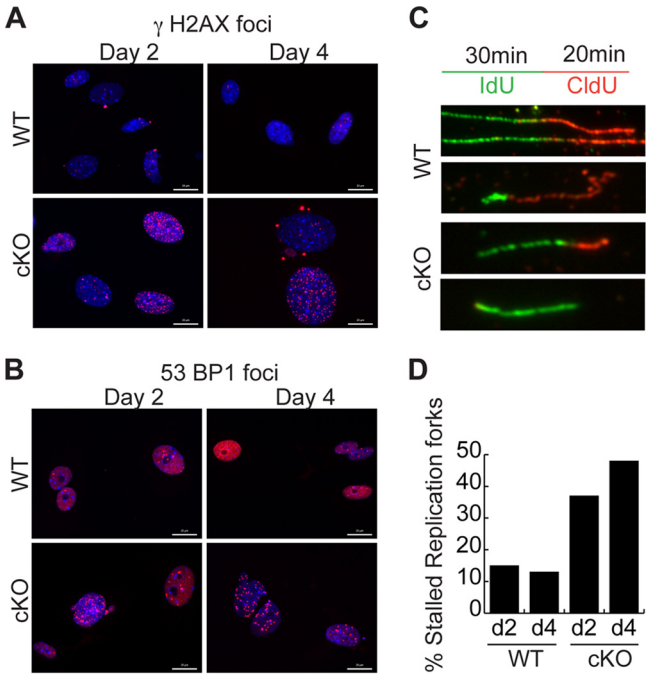

FIG 6 *Hinfp* is required for genomic stability and maintenance of DNA replication. WT and cKO MEFs were analyzed for factors associated with double-strand DNA damage by IF microscopy. (A) γ-H2AX S-139 (red); scale bar, 20 μm; (B) 53BP1 (red); scale bar, 20 μm. Nuclei were counterstained with DAPI (blue). cKO MEFs show a higher percentage of cells with both γ-H2AX and 53BP1 foci. (C) DNA fiber assay. WT and cKO MEFs were consecutively labeled with iododeoxyuridine (IdU; green) and chlorodeoxyuridine (CldU; red) at d2 and d4. Representative images of elongating and stalled forks are shown. *Hinfp*-null MEFs have a higher incidence of stalled replication forks than WT. (D) The bar graph represents percentage of stalled replication forks observed in WT and cKO MEFs at d2 and d4. There is increased frequency of stalled forks in *Hinfp*-null MEFs.

in *Hinfp*-deficient MEFs may also account for inhibition of cell proliferation and increased cellular senescence. Furthermore, increased nucleosome spacing may reduce the efficiency of periodic chromosome compaction and decondensation required for cell cycle progression. *Hinfp* loss creates multipolar mitotic spindles, suggesting defects in cytokinesis that result in altered genome content (e.g., aneuploidy and polyploidy). These changes in chromatin organization clarify the alterations in nuclear size and morphology observed in *Hinfp*-null cells. Collectively, our study demonstrates that *Hinfp*-dependent histone gene expression is essential for faithful replication and division of the genome.

Functional coupling between DNA replication and histone protein synthesis. Previous studies have established that histone protein synthesis is coupled to DNA replication and that inhibition of DNA synthesis acutely blocks histone protein synthesis (57–60). Here, we establish that a severe reduction in histone H4 expression impedes DNA synthesis and stalls replication forks. The altered nucleosome spacing caused by the unavailability of newly synthesized histone H4 may be responsible for fork stalling. Thus, the tight coupling between DNA replication and histone synthesis is reciprocal.

Collectively, our findings mechanistically elucidate a rate-limiting component of histone gene expression *in vivo* and firmly establish that *Hinfp* is a critical regulator of H4 genes. Our data are consistent with a coherent model in which loss of *Hinfp* deregulates the coupling between DNA synthesis and the packaging of newly replicated DNA. *Hinfp* deficiency reduces H4 gene expression and diminishes DNA replication fork progression, perhaps by inefficient deposition of histone H4 proteins. In interphase, these events may increase the mutation rate of genomic DNA and alter the distribution of epigenetic marks across the genome; in mitosis, chromosomal misalignments and genomic fragility may be increased. Thus, our results establish *Hinfp* as a central component of a molecular mechanism that maintains chromatin organization and genome integrity.

ACKNOWLEDGMENTS

This work was supported by Public Health Service grant R01 CA139322 from the National Institutes of Health.

We thank the members of our laboratory, especially Phil Tai for experimental expertise and Kaleem Zaidi for comments on the manuscript. We also thank Jaime Rivera and Jeanne Lawrence (Department of Cell and Developmental Biology, UMASS Medical School) for stimulating discussions and/or the sharing of expertise and reagents. We are grateful to Greg Pazour (Program in Molecular Medicine, UMASS Medical School) for providing the FLPeR mice. We acknowledge the assistance of the Core Flow Cytometry Lab at UMASS Medical School and the Flow Cytometry Facility at University of Vermont. We also thank Jennifer Díaz for help with manuscript preparation.

The contents of this report are solely the responsibility of the authors and do not necessarily represent the official views of the National Institutes of Health.

REFERENCES

1. **Luger K.** 2006. Dynamic nucleosomes. Chromosome Res. **14:**5–16. http://dx.doi.org/10.1007/s10577-005-1026-1.
2. **Wolffe A.** 1995. Chromatin: structure and function. Academic Press, London, United Kingdom.
3. **Stein GS.** 1984. Histone genes: structure, organization, and regulation. John Wiley & Sons, New York, NY.
4. **Plumb M, Stein J, Stein G.** 1983. Influence of DNA synthesis inhibition on the coordinate expression of core human histone genes during S phase. Nucleic Acids Res. **11:**7927–7945. http://dx.doi.org/10.1093/nar/11.22.7927.
5. **Sittman DB, Graves RA, Marzluff WF.** 1983. Histone mRNA concentrations are regulated at the level of transcription and mRNA degradation. Proc. Natl. Acad. Sci. U. S. A. **80:**1849–1853. http://dx.doi.org/10.1073/pnas.80.7.1849.
6. **Su C, Gao G, Schneider S, Helt C, Weiss C, O'Reilly MA, Bohmann D, Zhao J.** 2004. DNA damage induces downregulation of histone gene expression through the G_1 checkpoint pathway. EMBO J. **23:**1133–1143. http://dx.doi.org/10.1038/sj.emboj.7600120.
7. **Lichtler AC, Sierra F, Clark S, Wells JR, Stein JL, Stein GS.** 1982. Multiple H4 histone mRNAs of HeLa cells are encoded in different genes. Nature **298:**195–198. http://dx.doi.org/10.1038/298195a0.
8. **Braastad CD, Hovhannisyan H, van Wijnen AJ, Stein JL, Stein GS.** 2004. Functional characterization of a human histone gene cluster duplication. Gene **342:**35–40. http://dx.doi.org/10.1016/j.gene.2004.07.036.
9. **Medina R, Ghule PN, Cruzat F, Barutcu AR, Montecino M, Stein JL, van Wijnen AJ, Stein GS.** 2012. Epigenetic control of cell cycle-dependent histone gene expression is a principal component of the abbreviated pluripotent cell cycle. Mol. Cell. Biol. **32:**3860–3871. http://dx.doi.org/10.1128/MCB.00736-12.
10. **Hummon AB, Pitt JJ, Camps J, Emons G, Skube SB, Huppi K, Jones TL, Beissbarth T, Kramer F, Grade M, Difilippantonio MJ, Ried T, Caplen NJ.** 2012. Systems-wide RNAi analysis of CASP8AP2/FLASH shows transcriptional deregulation of the replication-dependent histone genes and extensive effects on the transcriptome of colorectal cancer cells. Mol. Cancer **11:**1. http://dx.doi.org/10.1186/1476-4598-11-1.
11. **Yang XC, Sabath I, Debski J, Kaus-Drobek M, Dadlez M, Marzluff WF, Dominski Z.** 2013. A complex containing the CPSF73 endonuclease and

other polyadenylation factors associates with U7 snRNP and is recruited to histone pre-mRNA for 3′-end processing. Mol. Cell. Biol. **33:**28–37. http://dx.doi.org/10.1128/MCB.00653-12.
12. **Stein GS, van Wijnen AJ, Stein JL, Lian JB, Montecino M, Zaidi SK, Braastad C.** 2006. An architectural perspective of cell-cycle control at the G_1/S phase cell-cycle transition. J. Cell Physiol. **209:**706–710. http://dx.doi.org/10.1002/jcp.20843.
13. **Muller B, Blackburn J, Feijoo C, Zhao X, Smythe C.** 2007. Are multiple checkpoint mediators involved in a checkpoint linking histone gene expression with DNA replication? Biochem. Soc. Trans. **35:**1369–1371. http://dx.doi.org/10.1042/BST0351369.
14. **Marzluff WF, Wagner EJ, Duronio RJ.** 2008. Metabolism and regulation of canonical histone mRNAs: life without a poly(A) tail. Nat. Rev. Genet. **9:**843–854. http://dx.doi.org/10.1038/nrg2438.
15. **Mitra P, Xie RL, Medina R, Hovhannisyan H, Zaidi SK, Wei Y, Harper JW, Stein JL, van Wijnen AJ, Stein GS.** 2003. Identification of HiNF-P, a key activator of cell cycle-controlled histone H4 genes at the onset of S phase. Mol. Cell. Biol. **23:**8110–8123. http://dx.doi.org/10.1128/MCB.23.22.8110-8123.2003.
16. **Holmes WF, Braastad CD, Mitra P, Hampe C, Doenecke D, Albig W, Stein JL, van Wijnen AJ, Stein GS.** 2005. Coordinate control and selective expression of the full complement of replication-dependent histone H4 genes in normal and cancer cells. J. Biol. Chem. **280:**37400–37407. http://dx.doi.org/10.1074/jbc.M506995200.
17. **Medina R, Buck T, Zaidi SK, Miele-Chamberland A, Lian JB, Stein JL, van Wijnen AJ, Stein GS.** 2008. The histone gene cell cycle regulator HiNF-P is a unique zinc finger transcription factor with a novel conserved auxiliary DNA-binding motif. Biochemistry **47:**11415–11423. http://dx.doi.org/10.1021/bi800961d.
18. **Miele A, Braastad CD, Holmes WF, Mitra P, Medina R, Xie R, Zaidi SK, Ye X, Wei Y, Harper JW, van Wijnen AJ, Stein JL, Stein GS.** 2005. HiNF-P directly links the cyclin E/CDK2/p220NPAT pathway to histone H4 gene regulation at the G_1/S phase cell cycle transition. Mol. Cell. Biol. **25:**6140–6153. http://dx.doi.org/10.1128/MCB.25.14.6140-6153.2005.
19. **Medina R, van Wijnen AJ, Stein GS, Stein JL.** 2006. The histone gene transcription factor HiNF-P stabilizes its cell cycle regulatory co-activator p220NPAT. Biochemistry **45:**15915–15920. http://dx.doi.org/10.1021/bi061425m.
20. **Zhao J, Dynlacht B, Imai T, Hori T, Harlow E.** 1998. Expression of NPAT, a novel substrate of cyclin E-CDK2, promotes S-phase entry. Genes Dev. **12:**456–461. http://dx.doi.org/10.1101/gad.12.4.456.
21. **Zhao J, Kennedy BK, Lawrence BD, Barbie DA, Matera AG, Fletcher JA, Harlow E.** 2000. NPAT links cyclin E-Cdk2 to the regulation of replication-dependent histone gene transcription. Genes Dev. **14:**2283–2297. http://dx.doi.org/10.1101/gad.827700.
22. **Ma T, Van Tine BA, Wei Y, Garrett MD, Nelson D, Adams PD, Wang J, Qin J, Chow LT, Harper JW.** 2000. Cell cycle-regulated phosphorylation of p220(NPAT) by cyclin E/Cdk2 in Cajal bodies promotes histone gene transcription. Genes Dev. **14:**2298–2313. http://dx.doi.org/10.1101/gad.829500.
23. **Ye X, Wei Y, Nalepa G, Harper JW.** 2003. The cyclin E/Cdk2 substrate p220(NPAT) is required for S-phase entry, histone gene expression, and Cajal body maintenance in human somatic cells. Mol. Cell. Biol. **23:**8586–8600. http://dx.doi.org/10.1128/MCB.23.23.8586-8600.2003.
24. **Ghule PN, Becker KA, Harper JW, Lian JB, Stein JL, van Wijnen AJ, Stein GS.** 2007. Cell cycle dependent phosphorylation and subnuclear organization of the histone gene regulator p220(NPAT) in human embryonic stem cells. J. Cell Physiol. **213:**9–17. http://dx.doi.org/10.1002/jcp.21119.
25. **Ghule PN, Dominski Z, Yang XC, Marzluff WF, Becker KA, Harper JW, Lian JB, Stein JL, van Wijnen AJ, Stein GS.** 2008. Staged assembly of histone gene expression machinery at subnuclear foci in the abbreviated cell cycle of human embryonic stem cells. Proc. Natl. Acad. Sci. U. S. A. **105:**16964–16969. http://dx.doi.org/10.1073/pnas.0809273105.
26. **Bongiorno-Borbone L, De Cola A, Vernole P, Finos L, Barcaroli D, Knight RA, Melino G, De Laurenzi V.** 2008. FLASH and NPAT positive but not coilin positive Cajal bodies correlate with cell ploidy. Cell Cycle **7:**2357–2367.
27. **Dominski Z, Marzluff WF.** 2007. Formation of the 3′ end of histone mRNA: getting closer to the end. Gene **396:**373–390. http://dx.doi.org/10.1016/j.gene.2007.04.021.
28. **Becker KA, Stein JL, Lian JB, van Wijnen AJ, Stein GS.** 2007. Establishment of histone gene regulation and cell cycle checkpoint control in human embryonic stem cells. J. Cell Physiol. **210:**517–526. http://dx.doi.org/10.1002/jcp.20903.
29. **Gao G, Bracken AP, Burkard K, Pasini D, Classon M, Attwooll C, Sagara M, Imai T, Helin K, Zhao J.** 2003. NPAT expression is regulated by E2F and is essential for cell cycle progression. Mol. Cell. Biol. **23:**2821–2833. http://dx.doi.org/10.1128/MCB.23.8.2821-2833.2003.
30. **Xie RL, Liu L, Mitra P, Stein JL, van Wijnen AJ, Stein GS.** 2007. Transcriptional activation of the histone nuclear factor P (HiNF-P) gene by HiNF-P and its cyclin E/CDK2 responsive co-factor p220NPAT defines a novel autoregulatory loop at the G_1/S phase transition. Gene **402:**94–102. http://dx.doi.org/10.1016/j.gene.2007.07.027.
31. **Xie R, Medina R, Zhang Y, Hussain S, Colby J, Ghule P, Sundararajan S, Keeler M, Liu LJ, van der Deen M, Mitra P, Lian JB, Rivera-Perez JA, Jones SN, Stein JL, van Wijnen AJ, Stein GS.** 2009. The histone gene activator HINFP is a nonredundant cyclin E/CDK2 effector during early embryonic cell cycles. Proc. Natl. Acad. Sci. U. S. A. **106:**12359–12364. http://dx.doi.org/10.1073/pnas.0905651106.
32. **Berthet C, Aleem E, Coppola V, Tessarollo L, Kaldis P.** 2003. Cdk2 knockout mice are viable. Curr. Biol. **13:**1775–1785. http://dx.doi.org/10.1016/j.cub.2003.09.024.
33. **Geng Y, Yu Q, Sicinska E, Das M, Schneider JE, Bhattacharya S, Rideout WM, Bronson RT, Gardner H, Sicinski P.** 2003. Cyclin E ablation in the mouse. Cell **114:**431–443. http://dx.doi.org/10.1016/S0092-8674(03)00645-7.
34. **Farley FW, Soriano P, Steffen LS, Dymecki SM.** 2000. Widespread recombinase expression using FLPeR (flipper) mice. Genesis **28:**106–110. http://dx.doi.org/10.1002/1526-968X(200011/12)28:3/4<106::AID-GENE30>3.0.CO;2-T.
35. **Byron M, Hall LL, Lawrence JB.** 2013. A multifaceted FISH approach to study endogenous RNAs and DNAs in native nuclear and cell structures. Curr. Protoc. Hum. Genet. Chapter 4:Unit 4.15. http://dx.doi.org/10.1002/0471142905.hg0415s76.
36. **Dimri GP, Lee X, Basile G, Acosta M, Scott G, Roskelley C, Medrano EE, Linskens M, Rubelj I, Pereira-Smith O, et al.** 1995. A biomarker that identifies senescent human cells in culture and in aging skin in vivo. Proc. Natl. Acad. Sci. U. S. A. **92:**9363–9367. http://dx.doi.org/10.1073/pnas.92.20.9363.
37. **Gotoh E.** 2009. Drug-induced premature chromosome condensation (PCC) protocols: cytogenetic approaches in mitotic chromosome and interphase chromatin. Methods Mol. Biol. **523:**83–92. http://dx.doi.org/10.1007/978-1-59745-190-1_6.
38. **Schwab RA, Niedzwiedz W.** 2011. Visualization of DNA replication in the vertebrate model system DT40 using the DNA fiber technique. J. Vis. Exp. e3255. http://dx.doi.org/10.3791/3255.
39. **Yokochi T, Gilbert DM.** 2007. Replication labeling with halogenated thymidine analogs. Curr. Protoc. Cell Biol. Chapter 22:Unit 22.10. http://dx.doi.org/10.1002/0471143030.cb2210s35.
40. **Solovei I, Schermelleh L, Albiez H, Cremer T.** 2006. Detection of the cell cycle stages *in situ* in growing cell populations, p 291–299. *In* Celis JE (ed), Cell biology: a laboratory handbook, 3rd ed, vol 1. Elsevier Academic Press, London, United Kingdom.
41. **Becker KA, Ghule PN, Therrien JA, Lian JB, Stein JL, van Wijnen AJ, Stein GS.** 2006. Self-renewal of human embryonic stem cells is supported by a shortened G_1 cell cycle phase. J. Cell Physiol. **209:**883–893. http://dx.doi.org/10.1002/jcp.20776.
42. **Stevens JB, Abdallah BY, Regan SM, Liu G, Bremer SW, Ye CJ, Heng HH.** 2010. Comparison of mitotic cell death by chromosome fragmentation to premature chromosome condensation. Mol. Cytogenet. **3:**20. http://dx.doi.org/10.1186/1755-8166-3-20.
43. **Francastel C, Schubeler D, Martin DI, Groudine M.** 2000. Nuclear compartmentalization and gene activity. Nat. Rev. Mol. Cell. Biol. **1:**137–143. http://dx.doi.org/10.1038/35040083.
44. **Woodcock CL, Skoultchi AI, Fan Y.** 2006. Role of linker histone in chromatin structure and function: H1 stoichiometry and nucleosome repeat length. Chromosome Res. **14:**17–25. http://dx.doi.org/10.1007/s10577-005-1024-3.
45. **Fernandez-Capetillo O, Chen HT, Celeste A, Ward I, Romanienko PJ, Morales JC, Naka K, Xia Z, Camerini-Otero RD, Motoyama N, Carpenter PB, Bonner WM, Chen J, Nussenzweig A.** 2002. DNA damage-induced G_2-M checkpoint activation by histone H2AX and 53BP1. Nat. Cell Biol. **4:**993–997. http://dx.doi.org/10.1038/ncb884.
46. **Anderson L, Henderson C, Adachi Y.** 2001. Phosphorylation and rapid

relocalization of 53BP1 to nuclear foci upon DNA damage. Mol. Cell. Biol. **21:**1719–1729. http://dx.doi.org/10.1128/MCB.21.5.1719-1729.2001.
47. **Price BD, D'Andrea AD.** 2013. Chromatin remodeling at DNA double-strand breaks. Cell **152:**1344–1354. http://dx.doi.org/10.1016/j.cell.2013.02.011.
48. **Liang D, Burkhart SL, Singh RK, Kabbaj MH, Gunjan A.** 2012. Histone dosage regulates DNA damage sensitivity in a checkpoint-independent manner by the homologous recombination pathway. Nucleic Acids Res. **40:**9604–9620. http://dx.doi.org/10.1093/nar/gks722.
49. **Smith MM, Stirling VB.** 1988. Histone H3 and H4 gene deletions in *Saccharomyces cerevisiae*. J. Cell Biol. **106:**557–566. http://dx.doi.org/10.1083/jcb.106.3.557.
50. **Kim UJ, Han M, Kayne P, Grunstein M.** 1988. Effects of histone H4 depletion on the cell cycle and transcription of *Saccharomyces cerevisiae*. EMBO J. **7:**2211–2219.
51. **Meeks-Wagner D, Hartwell LH.** 1986. Normal stoichiometry of histone dimer sets is necessary for high fidelity of mitotic chromosome transmission. Cell **44:**43–52. http://dx.doi.org/10.1016/0092-8674(86)90483-6.
52. **Prado F, Aguilera A.** 2005. Partial depletion of histone H4 increases homologous recombination-mediated genetic instability. Mol. Cell. Biol. **25:**1526–1536. http://dx.doi.org/10.1128/MCB.25.4.1526-1536.2005.
53. **Han M, Kim UJ, Kayne P, Grunstein M.** 1988. Depletion of histone H4 and nucleosomes activates the PHO5 gene in *Saccharomyces cerevisiae*. EMBO J. **7:**2221–2228.
54. **Clark-Adams CD, Norris D, Osley MA, Fassler JS, Winston F.** 1988. Changes in histone gene dosage alter transcription in yeast. Genes Dev. **2:**150–159. http://dx.doi.org/10.1101/gad.2.2.150.
55. **Zacchi LF, Selmecki AM, Berman J, Davis DA.** 2010. Low dosage of histone H4 leads to growth defects and morphological changes in *Candida albicans*. PLoS One **5:**e10629. http://dx.doi.org/10.1371/journal.pone.0010629.
56. **Tolstorukov MY, Sansam CG, Lu P, Koellhoffer EC, Helming KC, Alver BH, Tillman EJ, Evans JA, Wilson BG, Park PJ, Roberts CW.** 2013. Swi/Snf chromatin remodeling/tumor suppressor complex establishes nucleosome occupancy at target promoters. Proc. Natl. Acad. Sci. U. S. A. **110:**10165–10170. http://dx.doi.org/10.1073/pnas.1302209110.
57. **Baumbach LL, Marashi F, Plumb M, Stein G, Stein J.** 1984. Inhibition of DNA replication coordinately reduces cellular levels of core and H1 histone mRNAs: requirement for protein synthesis. Biochemistry **23:**1618–1625. http://dx.doi.org/10.1021/bi00303a006.
58. **Heintz N, Sive HL, Roeder RG.** 1983. Regulation of human histone gene expression: kinetics of accumulation and changes in the rate of synthesis and in the half-lives of individual histone mRNAs during the HeLa cell cycle. Mol. Cell. Biol. **3:**539–550.
59. **Helms S, Baumbach L, Stein G, Stein J.** 1984. Requirement of protein synthesis for the coupling of histone mRNA levels and DNA replication. FEBS Lett. **168:**65–69. http://dx.doi.org/10.1016/0014-5793(84)80207-0.
60. **Nelson DM, Ye X, Hall C, Santos H, Ma T, Kao GD, Yen TJ, Harper JW, Adams PD.** 2002. Coupling of DNA synthesis and histone synthesis in S phase independent of cyclin/cdk2 activity. Mol. Cell. Biol. **22:**7459–7472. http://dx.doi.org/10.1128/MCB.22.21.7459-7472.2002.